

Solketal Production in a Fixed Bed Adsorptive Reactor through the Ketalization of Glycerol

Miguel N. Moreira, Isabella Corrêa, Ana M. Ribeiro, Alírio E. Rodrigues, and Rui P. V. Faria*

Cite This: *Ind. Eng. Chem. Res.* 2020, 59, 2805–2816

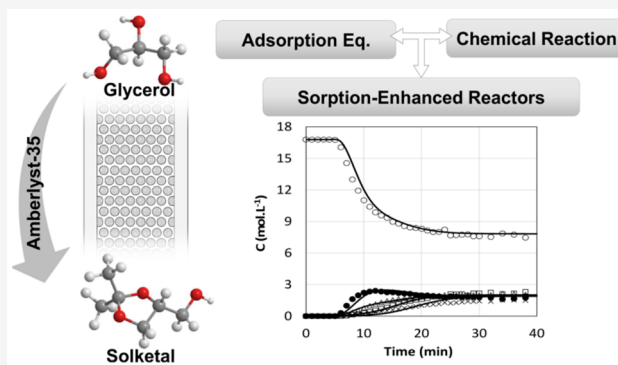
Read Online

ACCESS |

Metrics & More

Article Recommendations

ABSTRACT: Biodiesel production has been generating increasing amounts of glycerol as byproduct, therefore effective strategies are required to convert it into valuable chemicals to enhance the sustainability of the biodiesel production chain. In this work, solketal was synthesized by reacting glycerol with acetone (in the presence of ethanol) in a fixed bed adsorptive reactor packed with Amberlyst-35. Additionally, adsorption equilibrium isotherms for all the compounds of the process were determined at 313 K through a frontal analysis methodology, and the results were fitted through a competitive multicomponent Langmuir model. It was possible to conclude that water was the most adsorbed compound while solketal was the least. The potential for implementation of sorption-enhanced reactive processes was experimentally demonstrated since the conversion values transiently attained during the solketal synthesis process were approximately 30% above the equilibrium values. Finally, all the experimental results were accompanied by numerical simulation using a comprehensive mathematical model that was able to accurately describe the results.



1. INTRODUCTION

According to the International Energy Outlook 2017, global consumption of petroleum and other liquid fuels was 95 million barrels per day (b/d) in 2015, and expected to reach 104 million b/d in 2030,¹ with approximately 80% of the global energy generation deriving from fossil fuels.² Since 20% of the global energy consumption is used in the transportation sector,³ biodiesel is an attractive alternative to petrodiesel, once their calorific values are similar;⁴ it is renewable, nontoxic, and highly degradable; it produces no sulfur and no net CO₂ and releases less hydrocarbons and nongaseous emissions.⁵ The most common and widely accepted biodiesel production process is the catalyzed transesterification of triglycerides with an alcohol, producing esters (biodiesel) and glycerol (by-product).⁶ In terms of mass, glycerol is produced at a rate of 10% to biodiesel with a purity of 50–55%.⁷

One possible solution for this issue is to transform glycerol into other chemical commodities, such as fuel additives. One emergent fuel additive resulting from the glycerol ketalization reaction with acetone is solketal (4-hydroxymethyl-2,2-dimethyl-1,3-dioxolane), due to its ability to reduce gum formation and particle emission and to optimize the octane number when blended with gasoline. Furthermore, it is particularly interesting for the airline industry, once solketal can improve liquid properties for low temperature fuel transportation.^{8,9} Literature reports several works that study solketal synthesis through glycerol ketalization with acetone,

which generates water as byproduct, using various catalysts, such as zeolites,^{10,11} ion-exchange resins,^{12–14} and carbon materials,^{15,16} among others.^{14,17–20} According to the reaction stoichiometry, one mole of glycerol molecules will react with one mole of acetone molecules forming equimolar amounts of both products. The reaction is reversible and, therefore, the final conversion is determined by the thermodynamic equilibrium.¹²

Different technologies have also been proposed for the synthesis of this ketal. For instance, the production of solketal in a tubular reactor packed with Amberlyst-36 was proposed by Nanda et al.²¹ achieving a maximum solketal yield around 94% under optimum conditions. A similar process was proposed by Shirani et al.²² in which Puro-lite-PD206 was used as catalyst and subcritical acetone (at 20 °C and 120 bar) was used as the eluent and as a reactant, simultaneously. The authors reported a solketal yield of 95%. In both studies, the reactor outlet stream presented a low solketal concentration while considerable amounts of acetone (used as excess reactant) and water were also present in this stream. These two factors together will most probably lead to high downstream separation costs.

Received: November 28, 2019

Revised: January 21, 2020

Accepted: January 22, 2020

Published: January 22, 2020

Moreover, these two works focus on the optimization of the processes based on response surface methodologies without a detailed analysis of the physical–chemical phenomena underneath. Following alternative approaches, Clarkson et al.²³ and Roldán et al.²⁴ suggested the use of reactive distillation units and membrane reactors, respectively, for the production of solketal. Although the results obtained with these multifunctional reactors were satisfactory in terms of solketal yield (above 90% for both of the technologies studied), it is commonly acknowledged that distillation processes typically have high energy demands and zeolite membranes lack long-term stability, which might limit the application of these technologies at the industrial scale.

Despite the advances in the study of glycerol ketalization with acetone to produce solketal, some challenges on the purification step persist. In fact, it is known that this step can determine the commercial viability of an industrial process. Therefore, an entire industrial process can be discarded if the purification is not energetic and commercially viable.

Chromatography has proven to be efficient as a purification technology, finding applications over a wide range of fields, including the pharmaceutical, food, and petrochemical industries, for instance. The separation of the target compounds of complex multicomponent mixtures can be accomplished by taking advantage of the differences in the affinities of a solid stationary phase for the species present in a liquid mobile phase. Basically, compounds that develop stronger interaction with the solid material will percolate a chromatographic column at a lower speed than those that develop weaker interactions allowing the collection of purified fractions of the desired products. Hence, chromatographic separation can be accomplished in a large number of practical implementations and apparatus by selecting the adequate combination of mobile and stationary phases.²⁵

In the present work, the synthesis of solketal in a fixed bed adsorptive reactor was studied to evaluate the possibility of exploiting the synergetic effects arising from the combination of chromatographic separation with chemical reaction. The advantages reported for sorption-enhanced reactive processes for the synthesis of acetals,^{26–29} esters,^{30–33} and ethers,³⁴ among other organic compounds, will be similar to those attained when applying this technology to the ketalization of glycerol with acetone to produce this ketal. As suggested earlier, the selection of adequate stationary and mobile phases is a critical factor governing the performance of the process. Previous studies focused on the studied ketalization reaction suggest that the use of Amberlyst-35 and ethanol would represent one of the most promising solutions for the production of solketal through sorption-enhanced reactive processes.¹² In fact, in many of the examples previously provided regarding the application of fixed bed reactors to the synthesis of organic compounds, ion exchange resins, and Amberlyst-35 in particular, have been used as a stationary phase due to their ability to simultaneously act as adsorbent and catalyst for this sort of systems, presenting considerable adsorption selectivities and activity. On the other hand, ethanol is also widely used as the mobile phase in numerous chromatographic processes, does not react with the remainder species of the studied reactive system, and can be easily separated from the reaction products. Therefore, Amberlyst-35 and ethanol were selected as solid and liquid phases in this work.

Since sorption-enhanced reactive processes performance results from the contribution of several physical–chemical phenomena, namely, hydrodynamics, mass transfer, adsorption equilibrium, chemical reaction kinetics, and thermodynamic equilibrium, a comprehensive experimental work was performed, and complemented with mathematical modeling. Fundamental chemical reaction data have been previously determined and published in the open literature;¹² however, as far as our knowledge goes, this is the first study reporting adsorption equilibrium data for the species involved in the synthesis of solketal, a set of data strictly needed for the development of continuous sorption-enhanced reactive processes. Moreover, the feasibility of the technology was experimentally demonstrated highlighting the potential advantages of the combination of reaction and adsorption, through the analysis of the dynamics of the reactor. For that purpose, tracer experiments were performed for the characterization of the fixed bed column flow pattern, frontal analysis experiments were performed by sequentially feeding different mixtures of ethanol and one reactants or reaction products to determine the adsorption isotherms of all the species within this system at 313 K, and different reactive mixtures were fed to the fixed bed adsorptive reactor to produce solketal and study its dynamic behavior.

2. EXPERIMENTAL SECTION

2.1. Materials and Chemicals. To perform the experiments described in this section, glycerol (>99%) was purchased from Sigma-Aldrich, acetone (>99%) was purchased from Fisher Chemicals, solketal (>97%) was purchased from VWR International and ethanol (>99%) was purchased from Panreac-AppliChem. All the water used in this work was deionized in a two-bed deionization unit (assuring a conductivity lower than $1.0 \mu\text{S}\cdot\text{cm}^{-1}$), filtered, and degassed in our laboratories. Additionally, dimethyl sulfoxide (>99%) purchased from VWR International was used as an internal standard in the analytical method and blue dextran with a molecular weight of 2 000 000 purchased from Sigma-Aldrich was used as tracer.

Amberlyst-35 was used as stationary phase in the fixed bed adsorptive reactor since this highly acid macroporous ion exchange resins composed by a styrene divinylbenzene polymeric matrix functionalized with sulfonic groups can act as catalyst and adsorbent, simultaneously. The most relevant physical–chemical properties of Amberlyst-35 are presented in Table 1.

2.2. Analytical Method. All the samples collected during the experiments were analyzed in triplicate to evaluate the reproducibility of the composition determined in a gas chromatograph (DANI Master GC) equipped with a thermal conductivity detector. Helium was used as carrier gas and the

Table 1. Amberlyst-35 Physical–Chemical Properties

property	value
acidity (equiv·kg ⁻¹)	5.2
particle diameter (μm)	780
average pore diameter (nm)	30
particle porosity	0.396 ³⁵
tortuosity	4.1 ³⁶
surface area (m ² ·g ⁻¹)	34 ³⁵
solid density (kg·m ⁻³)	1542 ³⁵

compounds were separated in a ParaBondQ column (25 m, 0.53 mm i.d., film thickness of 10.0 μm). The sample injection volume was 2 μL , with a split ratio of 1:10, using dimethyl sulfoxide as internal standard. The injector temperature was set to 573.15 K, and the linear velocity inside the column was 40 $\text{cm}\cdot\text{s}^{-1}$. The column, initially at 423.15 K was heated at 5 $\text{K}\cdot\text{min}^{-1}$ up to 553.15 K, and this temperature was held constant for 1 min. The temperature of the detector was set to 573.15 K.

2.3. Experimental Procedure and Setup. The experimental setup used in this work consisted of a jacketed fixed-bed column (length, 11.5 cm; diameter, 2.6 cm), packed with 25.0 g of Amberlyst-35. Different mixtures were fed to the fixed column using a high-pressure liquid chromatographic pump and the temperature of the system was kept at 313 K by a thermostatic bath. The setup also comprised a six-port injection valve at the inlet of the fixed bed column and a sampling valve at its outlet.

A volume of 200 μL of a Blue Dextran solution (approximately 5 $\text{g}\cdot\text{L}^{-1}$) was injected in the fixed bed column for its characterization through tracer experiments. Ethanol was used as eluent at three different flow rates (2.0 $\text{mL}\cdot\text{min}^{-1}$, 5.0 $\text{mL}\cdot\text{min}^{-1}$, and 7.5 $\text{mL}\cdot\text{min}^{-1}$) and the outlet concentration history was recorded with an UV-vis detector.

A frontal analysis technique was applied in this work consisting in performing sequential step changes in the composition of the fixed bed feed mixture until the steady state was reached.³⁷ Basically, in the first experiment the fixed bed was saturated with the eluent (ethanol), and a binary mixture of known composition containing the eluent and one of the reactants or one of the products was fed to the unit. The outlet compositions evolution was measured and registered throughout time until no further changes were observed in these variables. At the reported operating conditions, steady-state was achieved after approximately 30 to 45 min. For this reason, each breakthrough experiment was carried out for at least 60 min. At this moment, the amount adsorbed in equilibrium with the feed mixture composition can be estimated through the global mass balance of the system. Then, a step change is performed in the feed composition and the procedure is repeated until a new steady state is reached. Each of these experiments will allow the determination of one point of the adsorption equilibrium isotherm. It is important to notice that, for multicomponent mixtures, the total concentration will depend on the relative molar amounts of each compound and the respective molar volumes. Therefore, when one varies the concentration value for one of the components, the others will also change their molar concentration, accordingly. Moreover, as all the compounds adsorb at some extent in the solid phase, it was not possible to measure the adsorption equilibrium isotherms for each compound isolated. Instead, competitive adsorption isotherms were determined.

To synthesize solketal in a fixed bed adsorptive reactor, ternary mixtures comprising the two reactants (acetone and glycerol) and the eluent (ethanol) were fed to a column presaturated with the eluent, monitoring the outlet concentration of the reactor throughout the entire experiment until the steady-state was achieved. Experiments were performed using two acetone-to-glycerol molar ratios (1.0 and 2.0) in the feed stream, which also contained 50% of eluent, on a molar basis. The operating temperature was set to 313 K, and the feed streamflow rate was 5.0 $\text{mL}\cdot\text{min}^{-1}$. Afterward, the reactor

bed was regenerated by feeding pure ethanol, and the outlet concentration profile was once again monitored.

3. MATHEMATICAL MODEL AND NUMERICAL SOLUTION

To predict the dynamic behavior of the fixed-bed adsorptive reactor, and the binary breakthrough curve experiments performed, a mathematical model was developed. The model considers the following assumptions:

- isothermal operation
- plug-flow model with axial dispersion and negligible radial dispersion
- constant packing porosity and bed length
- velocity variations due to changes in the bulk composition
- internal and external mass transfer resistances lumped into a global mass transfer coefficient
- multicomponent adsorption equilibrium described by the extended Langmuir isotherm model

The bulk and particle mass balance equations to component i are presented by eqs 1 and 2, respectively,

$$\frac{\partial C_i}{\partial t} + \frac{\partial(uC_i)}{\partial z} + \frac{1 - \varepsilon_b}{\varepsilon_b} \frac{3}{r_p} k_{L,i}(C_i - \bar{C}_{p,i}) = D_{ax} \frac{\partial}{\partial z} \left(C_T \frac{\partial x_i}{\partial z} \right) \quad (1)$$

$$\frac{3}{r_p} k_{L,i}(C_i - \bar{C}_{p,i}) = \varepsilon_p \frac{\partial \bar{C}_{p,i}}{\partial t} + (1 - \varepsilon_p) \frac{\partial \bar{q}_i}{\partial t} - \nu_i \frac{\rho_b}{(1 - \varepsilon_b)} \mathfrak{R}(\bar{C}_{p,i}) \quad (2)$$

where C_i , $\bar{C}_{p,i}$ and \bar{q}_i represent the bulk concentration, the average concentration in the particle pores, and the adsorbed concentration for component i , respectively, x_i is the molar fraction of component i , C_T is the total concentration in the liquid phase, u is the interstitial velocity, ε_b and ε_p are the bed and particle porosity, respectively, r_p is the particle radius, ρ_b is the density of the bulk, D_{ax} is the axial dispersion coefficient, $k_{L,i}$ is the global mass-transfer coefficient, t is time, and z is the axial coordinate. The variables ν_i and \mathfrak{R} in eq 2, are specifically related to the chemical reaction and represent the stoichiometric coefficient and the reaction rate value of component i based on the local intraparticle composition, respectively. In a previous work,¹² it was demonstrated that the reaction rate can be described by the Langmuir-Hinshelwood-Hougen-Watson law in terms of activities, a_i , according to eq 4.

$$\mathfrak{R} = k_c \frac{a_{\text{Ac}} a_{\text{Gly}} - \frac{a_{\text{Solk}} a_{\text{W}}}{K_{\text{eq}}}}{(1 + K_{\text{S,W}} a_{\text{W}})^2} \quad (3)$$

From the published data, one can estimate a value of 0.389 for the equilibrium constant, K_{eq} , a value of 492 $\text{mol}\cdot\text{kg}_{\text{cat}}^{-1}\cdot\text{s}^{-1}$ for the kinetic constant, k_c , and a value of 14.4 for the water adsorption constant, $K_{\text{S,W}}$, at 313 K. Note that the reaction rate was considered to be zero when simulating the experiments performed using only the eluent and one of the reactants or reaction products.

The total molar concentration in the bulk phase is calculated by eq 4 and depends on the local composition and the molar volume of each component, $V_{M,i}$.

$$C_T = \frac{1}{\sum x_i V_{M,i}} \quad (4)$$

The interstitial fluid velocity variation is given by eq 5, obtained from the global mass balance to the system.

$$\frac{du}{dz} = -\frac{1 - \varepsilon_b}{\varepsilon_b} \frac{3}{r_p} \sum_{i=1}^{NC} k_{L,i} V_{M,i} (C_i - \bar{C}_{p,i}) \quad (5)$$

Initial and Danckwerts boundary conditions are given by eqs 6 to 9,

$$t = 0 \quad C_i = \bar{C}_{p,i} = C_{i,0} \quad (6)$$

$$z = 0 \quad u C_{in,i} = u C_{i,z=0} - D_{ax} C_T \left. \frac{\partial x_i}{\partial z} \right|_{z=0} \quad (7)$$

$$z = 0 \quad u = u|_{z=0} \quad (8)$$

$$z = L \quad \left. \frac{\partial x_i}{\partial z} \right|_{z=L} = 0 \quad (9)$$

This model considers that a global mass-transfer coefficient combines external and internal mass-transfer coefficients, k_{ext} and k_{int} , respectively, according to the resistances-in-series model given by eq 10.

$$\frac{1}{k_L} = \frac{1}{k_{ext}} + \frac{1}{\varepsilon_p k_{int}} \quad (10)$$

The internal mass-transfer coefficient was estimated by eq 11,³⁸ while the external mass-transfer coefficient was estimated by the Wilson and Geankopolis³⁹ correlation, expressed by eq 12.

$$k_{int} = \frac{5D_m/\tau}{r_p} \quad (11)$$

$$Sh_p = \frac{1.09}{\varepsilon_p} (Re_p Sc)^{0.33}; \quad 0.0015 < Re_p < 55 \quad (12)$$

where D_m is the molecular diffusivity, τ is the particle tortuosity, Sh_p and Re_p are the Sherwood and Reynolds numbers relative to the particle, respectively, described by eqs 13 and 14, and Sc is the Schmidt number, which was determined according to eq 15.

$$Sh_p = \frac{k_{ext,i} 2r_p}{D_{i,m}} \quad (13)$$

$$Re_p = \frac{\rho 2r_p u}{\eta_m} \quad (14)$$

$$Sc = \frac{\eta}{\rho D_{i,m}} \quad (15)$$

In the previous equations, $D_{i,m}$ represents the diffusion coefficient of component i in a mixture. To compute these values, the infinite dilution diffusivities were first estimated through the Scheibel⁴⁰ correlation, eq 16,

$$D_{i,j}^0 = \frac{8.2 \times 10^{-8} T}{\eta_j V_{M,i}^{1/3}} \left[1 + \left(\frac{3V_{M,j}}{V_{M,i}} \right)^{2/3} \right] \quad (16)$$

where D_{ij}^0 is the diffusion coefficient for a dilute solute i in a solvent j , T is the temperature, and η_j is the viscosity of solvent j . Then, for multicomponent systems, the Perkins and Geankopolis⁴¹ correlation can be used to predict the molecular diffusivity coefficient of a compound in the mixture, $D_{i,m}$, eq 17,

$$D_{i,m} \eta_m^{0.8} = \sum_{\substack{j=1 \\ j \neq i}}^n x_j D_{i,j}^0 \eta_j^{0.8} \quad (17)$$

where η_m is the viscosity of the mixture and η_j is the viscosity of the component j . The effective diffusion coefficients, $D_{eff,i}$ are then estimated by eq 18.

$$D_{eff,i} = \frac{\varepsilon_p D_{i,m}}{\tau} \quad (18)$$

To complete the fixed bed adsorptive reactor model, the adsorption equilibrium of all the components was described by the multicomponent Langmuir adsorption equilibrium isotherm, eq 19.

$$\bar{q}_i = \frac{Q_i K_i \bar{C}_{p,i}}{1 + \sum_{j=1}^{NC} K_j \bar{C}_{p,j}} \quad (19)$$

In the previous equation, Q_i and K_i represent the monolayer capacity and the equilibrium constant for component i , respectively. The Langmuir adsorption equilibrium model has been widely applied to similar sorption-enhanced reactive processes,^{26–29} since it is simple to implement and provides an accurate description of the dependence of the adsorbed concentration as a function of the liquid concentration in this type of multicomponent systems; however, it is important to underline that it does not provide a phenomenological description of adsorption in ion exchange resins.

Finally, the numerical solution of these equations was accomplished with the assistance of the commercial software General PROcess Modeling System (gPROMS) version 4.2.0, using a method of orthogonal collocation in finite elements, and discretizing the axial dimension of the fixed bed column in 30 finite elements with two interior collocation points in each finite element. An integrated differential-algebraic equation solver (DASOLV) was then used to solve the system of ordinary differential equations in time.

4. RESULTS AND DISCUSSION

4.1. Hydrodynamics Study and Adsorption Isotherms Determination.

The main goal of the tracer experiments performed was to determine the fixed bed adsorptive reactor porosity and its Peclet number, which relates the convective and dispersive effects (in the axial direction) in the bed ($Pe = uL/D_{ax}$). As blue dextran presents a hydrodynamic diameter of approximately 50 nm,⁴² it is not expected to penetrate in Amberlyst-35 pores. Therefore, the mean residence time, \bar{t}_r , was determined from the first statistical moment of the residence time distribution curve, $E(t)$, measured at the outlet of the unit as a response to a pulse injection of the tracer species. The bed porosity could then be determined by dividing this value by the reactor space time, τ , and mean residence time value. Equation 20 was used to determine the residence time distribution, while its first moment was computed through eq 21.

$$E(t) = \frac{C_{\text{out}}(t)}{\int_0^{\infty} C_{\text{out}}(t) dt} \quad (20)$$

$$\bar{t}_r = \varepsilon_b \frac{V}{Q} = \int_0^{\infty} tE(t) dt \quad (21)$$

Since the dispersion is related to the variance of the residence time distribution curve, to determine the Peclet number, it was necessary to compute the second statistical moment of the curve, according to eq 22.

$$\sigma^2 = \int_0^{\infty} (t - \bar{t}_r)^2 E(t) dt = \frac{2}{Pe} \bar{t}_r^2 \quad (22)$$

The Peclet number and porosity values estimated through the tracer experiments are presented in Table 2.

Table 2. Peclet Number and Bed Porosity Values Estimated through Tracer Experiments Performed at Different Flow Rates

Q (mL·min ⁻¹)	ε_b	Pe
2.0	0.404 ± 0.002	110 ± 14
5.0	0.417 ± 0.001	112 ± 6
7.5	0.411 ± 0.001	129 ± 5

The average values determined for the porosity and Peclet number considering all the tracer experiments performed were 0.411 ± 0.005 and 116 ± 12, respectively. The estimated Peclet number is in line with the range of values presented in many works dealing with similar systems.^{29,43} It is important to mention that none of these variables showed a dependence on the flow rate value within the studied range of operating conditions (2.0 mL·min⁻¹ to 7.5 mL·min⁻¹).

To complete the hydrodynamics study, a comparison between the experimental residence time distribution curves and the model prediction was performed (Figure 1); however, as blue dextran only percolates the bed through the interparticle space, during the tracer experiments there was no mass transfer from the fluid to the solid phase, no adsorption, and no chemical reaction, and for that reason, the mass balance to the mobile phase initially described by eq 1 could be simplified as shown in eq 23.

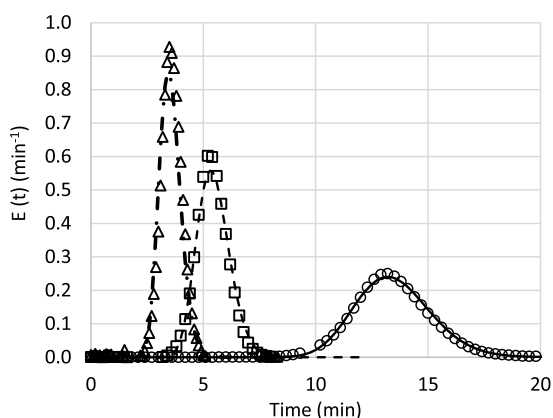


Figure 1. Residence time distribution determined for the tracer experiments. The symbols represent the experimental results at 2.0 mL·min⁻¹ (circles), 5.0 mL·min⁻¹ (squares), and 7.5 mL·min⁻¹ (triangles), and the lines represent the mathematical model prediction.

$$\frac{\partial C_i}{\partial t} + \frac{\partial(uC_i)}{\partial z} = D_{ax} \frac{\partial^2 C_i}{\partial z^2} \quad (23)$$

Figure 1 shows the good agreement between the experimental and simulated residence time distribution curves obtained through the tracer experiments.

After the full characterization of the bed and flow pattern, the study proceeded with the determination of fundamental adsorption data, namely, the adsorption isotherms for all the species involved in the synthesis of solketal. Although the open literature reports several methodologies for the estimation of multicomponent competitive adsorption isotherms,³⁷ including some specific for ion exchange resins based on the swelling of these materials in the presence of certain species,^{44–46} in this work the adsorption equilibrium parameters were assessed through the frontal analysis methodology, since it has been reported as one of the most reliable and expeditious procedures and it does not require any previous information regarding the adsorption equilibrium model.³⁷ Moreover, it has been thoroughly applied to similar systems with good results.^{26,27,29,47} As stated in the “Experimental Procedure and Setup” section, the frontal analysis technique consists in feeding a mixture of known composition to a fixed bed previously saturated with another mixture, until it becomes saturated with the new feed. If the initial composition of the bed is known, then the composition of the solid phase in equilibrium with the liquid phase can be estimated through the global mass balance of the system described by eqs 24 and 25, which allow the computation of the molar amount adsorbed in or desorbed from the solid phase, $n_{\text{ads/des}}$ when going from one equilibrium point to the other.

$$n_{\text{ads/des},i} = Q \int_0^t \alpha_i (C_{\text{in},i} - C_{i|z=L}) dt \quad (24)$$

$$\frac{n_{\text{ads/des},i} \alpha_i}{V} = (\varepsilon_b + (1 - \varepsilon_b) \varepsilon_p) (C_{\text{in},i} - C_{0,i}) + (1 - \varepsilon_b) (1 - \varepsilon_p) (q_{\text{in},i} - q_{0,i}) \quad (25)$$

The variable Q represents the experimental flow rate value, α_i is a coefficient that takes a value of 1 or -1 depending on if the species is being adsorbed or desorbed, respectively, V is the fixed bed column volume, and the variables $C_{0,i}$, $C_{\text{in},i}$, $q_{0,i}$ and $q_{\text{in},i}$ represent the initial and inlet concentration of compound i in the liquid phase and the concentration of compound i in the solid phase in equilibrium with the two previous liquid phase concentration values, respectively.

With this, it is possible to determine the adsorption equilibrium isotherm for each species; however, it is important to underline that, as this is a reactive system, the experiments always had to be performed using nonreactive binary mixtures composed by the eluent (ethanol) and one of the reactants or the products. Then, the adsorption equilibrium results were fitted to a multicomponent competitive Langmuir adsorption model considering all the breakthrough experiments performed and using Matlab’s integrated solver, *fminsearch*, to minimize the sum of the residuals between the experimental adsorbed concentration values and the values determined by the selected adsorption isotherm model, setting a convergence tolerance of 10⁻⁵. The errors associated with the parameters were estimated through the Bootstrap methodology (resampling the residuals and using 2000 bootstrap repetitions).^{48,49} However, instead of estimating the parameters Q_i and K_i from eq 19, an approach

reported by previous authors was followed,³⁰ in which the monolayer adsorption capacity for each species is a function of its molar volume ($Q_i = Q_v/V_{M,i}$) so that a single value, Q_v , can be assumed for the capacity of the adsorbent. It is explained by the fact that the assumption of a maximum monolayer adsorption molar capacity proposed by the Langmuir model is typically not verified for highly concentrated systems composed of molecules with very different sizes.²⁶ This strategy will not only reduce the number of parameters to be estimated, and therefore reduce the errors associated with its estimation, but it will also improve the consistency of the results. Table 3 presents the estimated parameters. Figure 2 to

Table 3. Molar Volumes and Multicomponent Langmuir Adsorption Equilibrium Parameters of the Species Involved in the Synthesis of Solketal in Amberlyst-35 at 313 K

compound	$V_{M,i}$ (L·mol ⁻¹)	Q_v (L·L _{Ads} ⁻¹)	Q_i (mol·L _{Ads} ⁻¹)	K_i (L·mol ⁻¹)
acetone	75.6	0.414 ± 0.005	5.48 ± 0.06	3.58 ± 0.70
glycerol	73.8		5.61 ± 0.07	44.7 ± 3.9
solketal	115.5		3.58 ± 0.04	2.08 ± 0.69
water	18.0		23.0 ± 0.3	47.4 ± 4.8
ethanol	59.6		6.95 ± 0.08	15.2 ± 1.48

Figure 5 provide a comparison between the adsorbed concentrations predicted by the Langmuir isotherm with those parameters and the values determined experimentally.

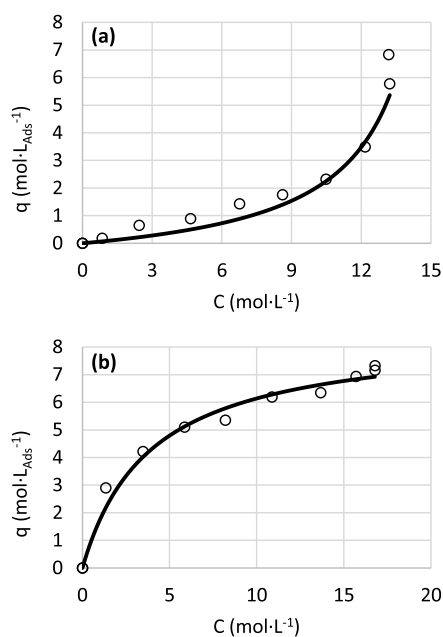


Figure 2. Langmuir competitive adsorption isotherms for binary mixtures of acetone (a) and ethanol (b) over Amberlyst-35 at 313 K. The dots represent the experimental results and the lines represent the mathematical model prediction ($R^2 = 0.943$ for acetone).

The results show that the competitive multicomponent Langmuir model can accurately describe the experimentally determined adsorption isotherms. Nevertheless, one should be aware that it does not provide a phenomenological description of the phenomena. Instead, it represents a reasonable approximation that is able to fit the experimental data. It is important to highlight again that the parameter estimation was

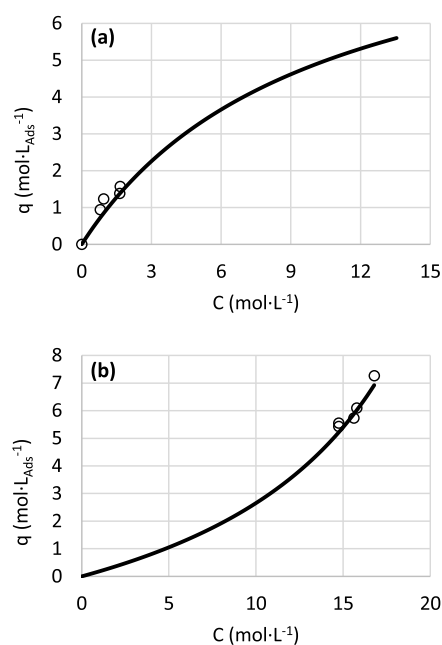


Figure 3. Langmuir competitive adsorption isotherms for binary mixtures of glycerol (a) and ethanol (b) over Amberlyst-35 at 313 K. The dots represent the experimental results and the lines represent the mathematical model prediction ($R^2 = 0.847$ for glycerol).

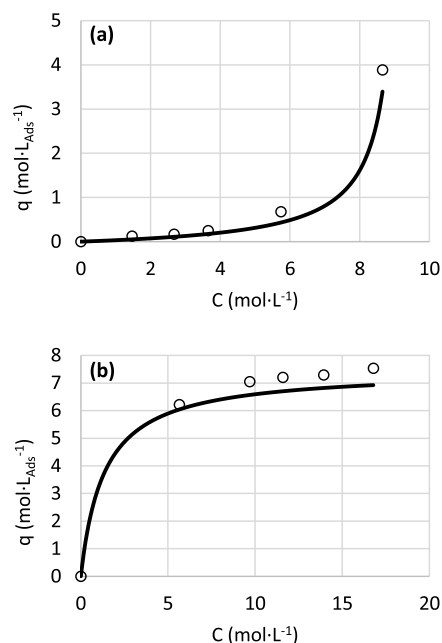


Figure 4. Langmuir competitive adsorption isotherms for binary mixtures of solketal (a) and ethanol (b) over Amberlyst-35 at 313 K. The dots represent the experimental results and the lines represent the mathematical model prediction ($R^2 = 0.972$ for solketal).

not performed individually for each binary mixture. Instead, all the binary competitive adsorption isotherm parameters were estimated simultaneously. The main reason for this is related to ethanol which was present in all binary systems. If the parameter estimation was made independently, four different sets of parameters would be obtained for ethanol while, through the procedure adopted, only one set of parameters was estimated ($R^2 = 0.984$ for ethanol, considering all binary systems). Although this might lead to slightly higher deviations

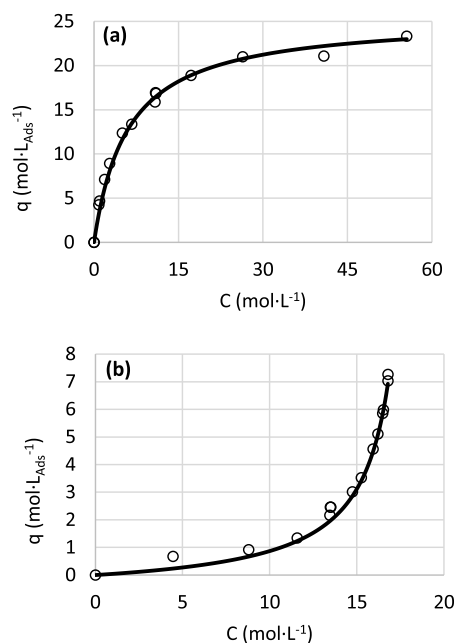


Figure 5. Langmuir competitive adsorption isotherms for binary mixtures of water (a) and ethanol (b) over Amberlyst-35 at 313 K. The dots represent the experimental results and the lines represent the mathematical model prediction ($R^2 = 0.991$ for water).

for some of the binary systems (as those observed in Figure 4a, for ethanol concentrations above $10 \text{ mol}\cdot\text{L}^{-1}$), this procedure will increase the reliability of the adsorption parameters estimated and provide a better description of the adsorption equilibrium in more complex multicomponent mixtures. The largest deviations are observed for glycerol, which are probably due to quantification issues and to its transport properties (high viscosity, high density, low mass transfer coefficient) which make the practical implementation of the frontal analysis method more difficult. The results also show that, as expected, water is the most adsorbed species for the selected solid stationary phase while solketal is the least adsorbed one. Ethanol, on the other hand, seems to adsorb considerably less than water and more than solketal. The combination of all these factors is particularly favorable for the implementation of sorption-enhanced reactive processes, since high selectivity between products can increase the process productivity, while using an eluent with intermediate adsorption properties will reduce the eluent consumption.

To perform a first assessment of the reliability of the mathematical model described in section 3, all the binary breakthrough experiments performed with nonreactive pairs were simulated considering the previously estimated parameters. A comparison between the experimental data and simulation results for each binary is presented in Figure 6 to Figure 9, and the coefficient of determination, R^2 , computed through eq 26, was used for a quantitative analysis of the quality of the fitting.

$$R^2 = 1 - \frac{\sum_i^{NC} \sum_j^{NP} (C_{ij}^{\text{exp}} - C_{ij}^{\text{model}})^2}{\sum_i^{NC} \sum_j^{NP} (C_{ij,k}^{\text{exp}} - \bar{C}_i)^2} \quad (26)$$

The variables NC and NP represent the number of compounds and experimental data points, C_{ij}^{exp} and C_{ij}^{model} , represent the experimental and predicted outlet concentration for compound

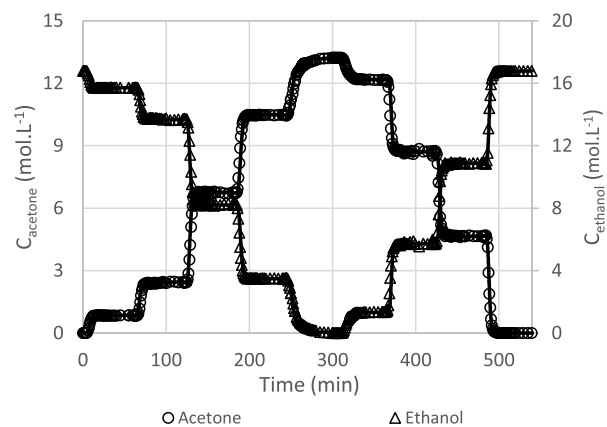


Figure 6. Experimental and predicted outlet concentration histories for the breakthrough curves performed with binary mixtures of acetone and ethanol at 313 K and $5.0 \text{ mL}\cdot\text{min}^{-1}$ ($R^2 = 0.998$).

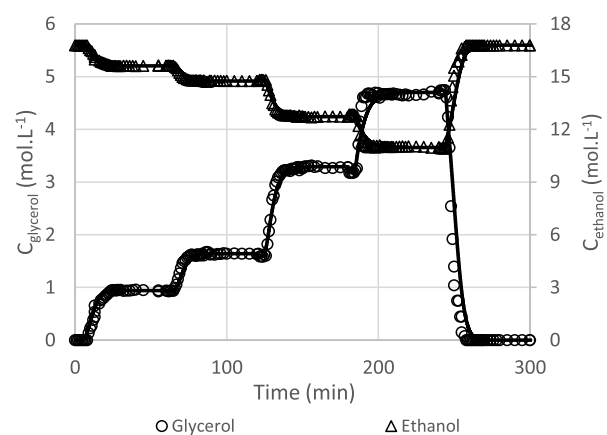


Figure 7. Experimental and predicted outlet concentration histories for the breakthrough curves performed with binary mixtures of glycerol and ethanol at 313 K and $5.0 \text{ mL}\cdot\text{min}^{-1}$ ($R^2 = 0.981$).

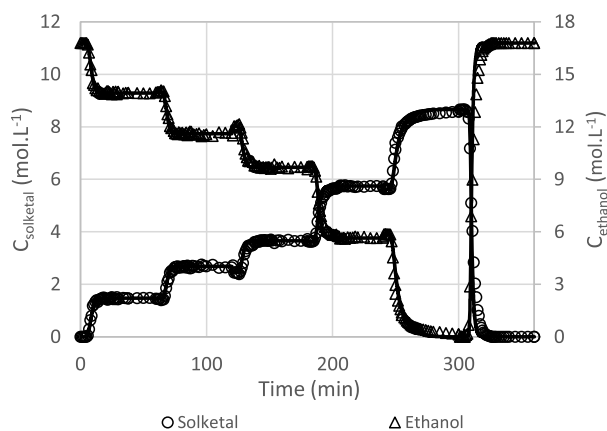


Figure 8. Experimental and predicted outlet concentration histories for the breakthrough curves performed with binary mixtures of solketal and ethanol at 313 K and $5.0 \text{ mL}\cdot\text{min}^{-1}$ ($R^2 = 0.993$).

i in the j th data point. \bar{C}_i is the average concentration value of compound i considering all data points.

The analysis of the results reported in Figure 6 to Figure 9 suggests that the model is able to predict the dynamic behavior of the adsorptive bed with reasonably high accuracy. The average retention times determined from the experimental and

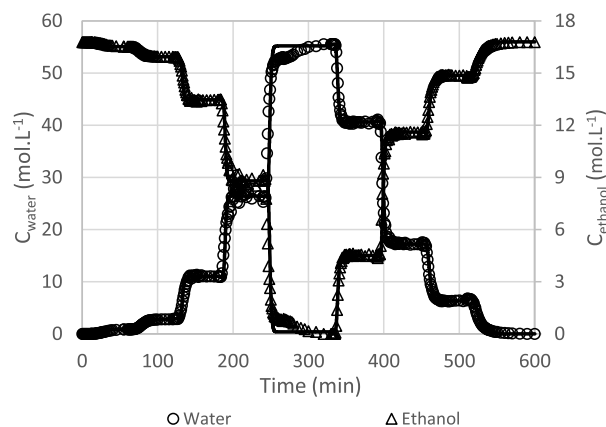


Figure 9. Experimental and predicted outlet concentration histories for the breakthrough curves performed with binary mixtures of water and ethanol at 313 K and 5.0 mL·min⁻¹ ($R^2 = 0.993$).

simulated data are in good agreement for all the breakthrough experiments performed and the dispersive effects that result from the mass transfer phenomena, as well as from the adsorption equilibrium, could be well fitted by the mathematical model. These statements are supported by the high values determined for the coefficient of determination for the acetone–ethanol, glycerol–ethanol, solketal–ethanol, and water–ethanol breakthrough experiments: 0.998, 0.981, 0.993, and 0.993, respectively.

4.2. Solketal Synthesis Experiments and Simulations.

To accomplish the synthesis of solketal in a fixed bed adsorptive reactor and to study its dynamic behavior, a reactive mixture composed of acetone and glycerol in a 1:1 molar ratio was diluted in 50% of ethanol (molar basis) and fed at 5.0 mL·min⁻¹ to a reactor operated at 313 K, which was initially saturated with the eluent. The resulting outlet concentration histories are presented in Figure 10.

The results demonstrate that the fixed bed adsorptive reactor packed with Amberlyst-35 was able to convert the reactants and produce solketal as desired. A more detailed analysis of the dynamics of the reactor verifies that solketal was the first species to elute from the reactor, after approximately 5 min, while water was the last species to be detected at its outlet (3 min later). These observations are in line with the adsorption parameters determined in the previous section which indicated that solketal and water are, respectively, the least and most adsorbed species in Amberlyst-35. As reaction proceeded and the bed became saturated with water, the outlet concentration values kept changing until the steady state was reached, at the end of approximately 35 min. As expected, considering the reaction stoichiometry and the feed mixture composition, equivalent amounts of the two reactants were attained at this point and the same was observed for the products. During the desorption step, it was also observed that all the species eluted from the reactor according to their affinity toward the resin: first solketal, followed by acetone, glycerol, and finally water. Approximately 400 mL of ethanol was required for the regeneration of the fixed bed due to the highly dispersive behavior of the water desorption band.

One of the most important findings of the present work was the experimental demonstration of the potential for implementing sorption-enhanced reactive processes for the synthesis of solketal based on the mobile and stationary phases selected. As one can observe from Figure 10, the concentration of

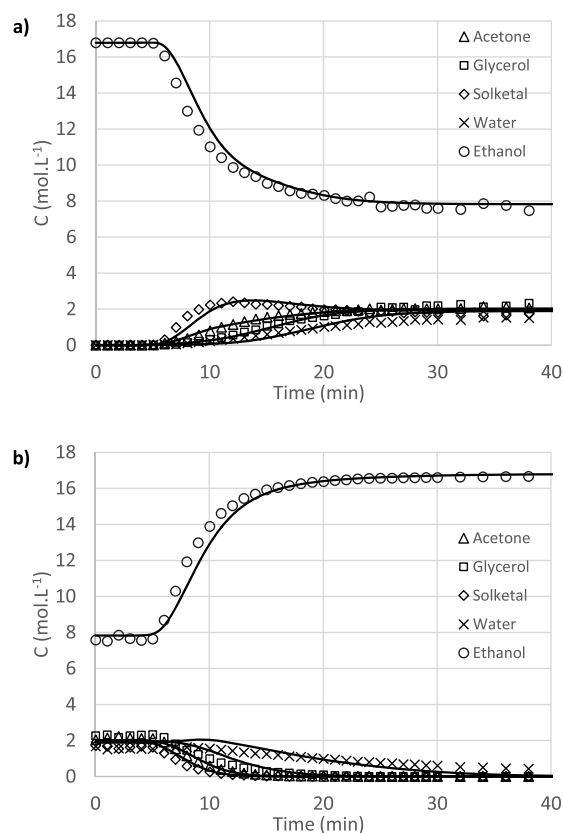


Figure 10. Outlet concentration histories (a) of a fixed bed adsorptive reactor operated at 313 K for the synthesis of solketal by feeding acetone and glycerol (molar ratio of 1.0) diluted in 50% of ethanol (molar basis) at 5.0 mL·min⁻¹ and (b) outlet concentration histories for the regeneration of the reactor with a pure ethanol stream at the same flow rate.

solketal reached a maximum value of 2.4 mol·L⁻¹ (12.0 min) before stabilizing at 1.7 mol·L⁻¹ at the steady state. This means that, by taking advantage of the synergetic effects of adsorption and reaction when those two phenomena occur simultaneously in the same unit, it is possible to temporarily overcome the thermodynamic equilibrium conversion (estimated as 49% according to previous works¹²) by approximately 30%. Under the studied operating conditions, the maximum experimental conversion registered was 63% and the experimental steady state conversion was 43%.

In order to increase the conversion and to validate the mathematical model under a wider range of conditions, solketal was synthesized using an acetone-to-glycerol molar ratio of 2.0. Figure 11 presents the outlet concentration histories obtained under these conditions.

Similar trends were observed for experiments performed by feeding a stoichiometric mixture or acetone in excess. The compounds elution order remained the same, and the steady state was reached after 35 min as well. However, higher conversions were attained when using uneven amounts of reactants, as expected. In fact, the steady state conversion increased to 62% almost reaching the equilibrium conversion (66%). Since the provided contact time between the reactants and the catalyst should be enough to reach the reaction equilibrium conversion, the slight deviation between the two values can be attributed to the quantification method. Moreover, the enhancement of the conversion through the

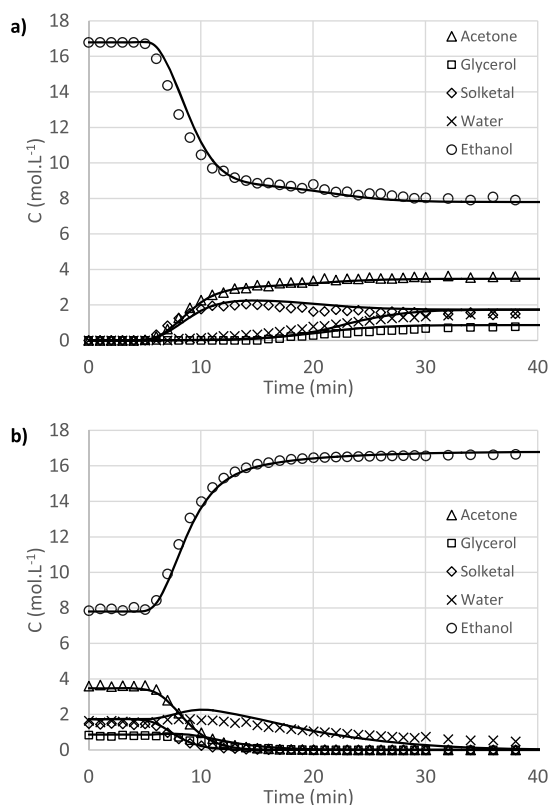


Figure 11. Outlet concentration histories (a) of a fixed bed adsorptive reactor operated at 313 K for the synthesis of solketal by feeding acetone and glycerol (molar ratio of 2.0) diluted in 50% of ethanol (molar basis) at $5.0 \text{ mL}\cdot\text{min}^{-1}$ and (b) outlet concentration histories for the regeneration of the reactor with a pure ethanol stream at the same flow rate.

integration of adsorption and reaction in this unit was again evidenced by the roll-up in the solketal outlet concentration history. The maximum concentration and conversion values registered experimentally were $2.0 \text{ mol}\cdot\text{L}^{-1}$ and 81% (14.0 min), respectively.

Finally, another relevant output from this work is the fact that the developed model and the estimated adsorption parameters were able to fit the experimental data with considerable accuracy, for both the reaction and regeneration steps and regardless of the feed composition. The coefficients of determination computed for the first and the second experiments were 0.959 and 0.974, respectively. The most significant deviations between the model and the experimental data were observed for water desorption curves which presented a considerably higher dispersion than the one predicted by the model. This can be related with the swelling and shrinking of the ion-exchange resin during the process, which might change the packing and the dispersion coefficients estimated through the tracer experiments performed. Nevertheless, the results suggest that the model can be used as a reliable starting point for the development of more complex and continuous sorption-enhanced reactive processes for the synthesis of solketal.

In this context, a simple modeling study was performed to assess the effect of some relevant variables in the fixed bed adsorptive reactor performance, namely, the feed flow rate, and to evaluate the possibility of using technical grade glycerol in the feed stream.

Changing the feed flow rate will have a direct impact in the contact time between the reactive species and the catalyst, which will affect the reaction extension. The effect of the flow rate in the fixed bed adsorptive reactor steady-state conversion and maximum conversion is presented in Figure 12,

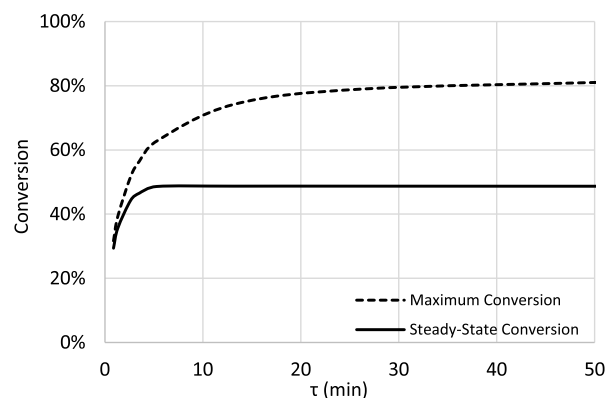


Figure 12. Effect of space time on the maximum and steady state conversions attained in the fixed bed adsorptive reactor at 313 K, feeding equimolar amounts of glycerol and acetone diluted in 50% of ethanol.

considering as case study a feed mixture composed by equimolar amounts of acetone and glycerol diluted in 50% of eluent (similar to the first fixed bed adsorptive reactor experiment).

The results demonstrate that for space time values higher than 5 min the equilibrium conversion for an equimolar mixture of glycerol and acetone diluted in 50% of ethanol at 313 K can be reached. Moreover, maximum conversion values above 75% can be transiently achieved if a space time higher than 15 min is provided (against the 49% conversion limit imposed by the thermodynamic equilibrium). Note that, although the operating temperature can have a significant impact on the fixed bed reactor conversion as well, this issue could not be addressed because the adsorption parameters were only determined for 313 K and, for this reason, the dependence of these variables with temperature could not be accounted for in the mathematical model. The advantages of synthesizing solketal through a sorption-enhanced reactive process become once again evident through the results presented in Figure 12.

To evaluate the possibility of using technical grade glycerol instead of synthetic glycerol, several simulations were performed considering different amounts of water in the feed mixture, since 6 wt % to 8 wt % of water is typically present in technical grade glycerol. For that purpose, the same flow rate, temperature, reactants molar ratio, and solvent amount as in the first fixed bed adsorptive reactor experiment was assumed. As widely known, adding one of the products to a reactive mixture will decrease the limiting reactant conversion. As a direct consequence, the steady state conversion of the fixed bed adsorptive reactor dropped to 39% and 37% by feeding glycerol containing 6 wt % and 8 wt % of water, respectively. Even the addition of a water amount as low as 2 wt % (relative to the glycerol weight) would lead to a decline on the steady state conversion from 49% to 44%, approximately. On the other hand, the use of technical grade glycerol seems to have a less significant impact on the maximum conversion achieved at the outlet of the fixed bed reactor. In the worst-case scenario

tested, that is, glycerol containing 8 wt % of water, the maximum conversion decreased to 55% which is still above the equilibrium conversion at these conditions (approximately 49%). If the water content introduced in the fed glycerol is lower than 2 wt% then a decrease of only 1% is observed for the maximum conversion. The high selectivity of the selected catalyst/adsorbent (Amberlyst-35) between water and solketal allows the concentration front of the target product to travel much faster through the bed while water is preferably adsorbed and retained by the solid phase. In this way, the maximum conversion is less affected by the presence of the byproduct in the feed mixture.

5. CONCLUSIONS

The main goal of the present work was to synthesize solketal in a fixed bed adsorptive reactor packed with Amberlyst-35 through the ketalization of glycerol with acetone, and to analyze the dynamic behavior of this unit in order to evaluate its sorption enhancement potential.

For that purpose, fundamental adsorption equilibrium had to be determined. A frontal analysis methodology was applied using nonreactive binary mixtures composed by one of the reactants or one of the products and ethanol, which was used as eluent in this process. At 313 K and within the studied concentration ranges, the experimental results could be well fitted by a multicomponent competitive Langmuir adsorption model. The estimated adsorption constant values for acetone, glycerol, solketal, water, and ethanol were 3.58 ± 0.70 , 44.7 ± 3.9 , 2.08 ± 0.69 , 47.4 ± 4.8 , and 15.2 ± 1.48 , respectively while their maximum capacities were 5.48 ± 0.06 , 5.61 ± 0.07 , 3.58 ± 0.04 , 23.0 ± 0.3 , and 6.95 ± 0.08 (in the same order). From these results, it was possible to verify that water is the most adsorbed compound, as expected for highly acid cation exchange resins, while solketal was the least adsorbed compound. The fundamental adsorption data determined in this work is crucial for the development of sorption-enhanced reactive processes for the synthesis of solketal based on this mobile and stationary phases, and the information previously published in the open literature regarding this topic was scarce or inexistent.

The experimental results obtained demonstrated that solketal can indeed be produced in a fixed bed adsorptive reactor at 313 K. The steady state limiting reactant conversions attained by feeding stoichiometric amounts of the reactants or an excess of acetone (at a molar ratio of 2.0) were 43% and 62%, respectively; however, considerably higher conversion values were attained during the operation. When using an acetone to glycerol molar ratio of 1.0 the conversion reached 63% while a molar ratio of 2.0 allowed to achieve a conversion of 81%. These results are a clear demonstration that the integration of adsorption and reaction in a single unit can lead to important improvements on the reactors performance for this system through the implementation of the adequate sorption enhanced reactive technology.

AUTHOR INFORMATION

Corresponding Author

Rui P. V. Faria – Laboratory of Separation and Reaction Engineering—Laboratory of Catalysis and Materials (LSRE-LCM), Department of Chemical Engineering, Faculty of Engineering, University of Porto 4200-465 Porto, Portugal; orcid.org/0000-0002-1216-0613; Phone: +351 22 508 1578; Email: rui.faria@fe.up.pt

Authors

Miguel N. Moreira – Laboratory of Separation and Reaction Engineering—Laboratory of Catalysis and Materials (LSRE-LCM), Department of Chemical Engineering, Faculty of Engineering, University of Porto 4200-465 Porto, Portugal

Isabella Corrêa – Laboratory of Separation and Reaction Engineering—Laboratory of Catalysis and Materials (LSRE-LCM), Department of Chemical Engineering, Faculty of Engineering, University of Porto 4200-465 Porto, Portugal

Ana M. Ribeiro – Laboratory of Separation and Reaction Engineering—Laboratory of Catalysis and Materials (LSRE-LCM), Department of Chemical Engineering, Faculty of Engineering, University of Porto 4200-465 Porto, Portugal; orcid.org/0000-0003-4269-1420

Alírio E. Rodrigues – Laboratory of Separation and Reaction Engineering—Laboratory of Catalysis and Materials (LSRE-LCM), Department of Chemical Engineering, Faculty of Engineering, University of Porto 4200-465 Porto, Portugal; orcid.org/0000-0002-0715-4761

Complete contact information is available at: <https://pubs.acs.org/10.1021/acs.iecr.9b06547>

Notes

The authors declare no competing financial interest.

ACKNOWLEDGMENTS

This work was financially supported by Project PTDC/QEQ-ERQ/2698/2014—POCI-01-0145-FEDER-016866, funded by FEDER funds through COMPETE2020-Programa Operacional Competitividade e Internacionalização (POCI) and by national funds through FCT—Fundação para a Ciência e a Tecnologia, I.P.; NORTE-01-0145-FEDER-000006, funded by NORTE2020 through PT2020 and ERDF; Base Funding—UIDB/50020/2020 of the Associate Laboratory LSRE-LCM—funded by national funds through FCT/MCTES (PIDDAC).

NOTATION

Variables

- a_i = activity coefficient of compound i
- C_i = concentration of component i in the liquid phase mol L^{-1}
- $\bar{C}_{p,i}$ = average concentration in the particle pores of component i mol L^{-1}
- $C_{i,0}$ = initial concentration of compound i in the liquid phase mol L^{-1}
- $C_{in,i}$ = inlet concentration of compound i mol L^{-1}
- C_{out} = outlet concentration mol L^{-1}
- C_T = total concentration in the liquid phase mol L^{-1}
- D_{ax} = axial dispersion coefficient $\text{cm}^2 \text{s}^{-1}$
- $D_{eff,i}$ = effective diffusion coefficient $\text{cm}^2 \text{s}^{-1}$
- $D_{i,m}$ = diffusion coefficient of component i in a mixture $\text{cm}^2 \text{s}^{-1}$
- D_{ij}^0 = diffusion coefficient for a dilute solute i in a solvent j $\text{cm}^2 \text{s}^{-1}$
- D_m = molecular diffusivity $\text{cm}^2 \text{s}^{-1}$
- E = residence time distribution s^{-1}
- k_c = reaction kinetic constant $\text{mol kg}^{-1} \text{s}^{-1}$
- K_{eq} = reaction thermodynamic equilibrium constant
- $k_{ext,i}$ = external mass transfer coefficient of compound i cm s^{-1}

K_i = Langmuir adsorption equilibrium constant for compound i L mol⁻¹
 $k_{int,i}$ = internal mass transfer coefficient of compound i cm s⁻¹
 $k_{L,i}$ = global mass transfer coefficient of compound i cm s⁻¹
 $K_{S,W}$ = adsorption equilibrium constant for water (rate law) –
 L = fixed bed length cm
 $n_{ads/des,i}$ = Adsorbed/desorbed amount of compound i mol
 NC = number of compounds –
 NP = number of experimental data points –
 Pe = Peclet number –
 Q = flow rate L min⁻¹
 Q_i = Langmuir maximum capacity for compound i mol L_{Ads}⁻¹
 $q_{i,0}$ = initial concentration of compound i in the liquid phase mol L_{Ads}⁻¹
 $q_{in,i}$ = adsorbed concentration of compound i in equilibrium with the feed concentration mol L_{Ads}⁻¹
 \bar{q}_i = average adsorbed concentration of compound i mol L_{Ads}⁻¹
 Q_v = Langmuir capacity normalized by the molar volume L L_{Ads}⁻¹
 \mathcal{R} = reaction rate mol kg⁻¹ s⁻¹
 Re_p = Reynolds number (particle) –
 r_p = particle radius cm
 Sc = Schmidt number –
 Sh_p = Sherwood number (particle) –
 T = temperature K
 t = time s
 \bar{t}_r = average residence time s
 u = interstitial velocity cm s⁻¹
 V = fixed bed volume L
 $V_{M,i}$ = molar volume of compound i L mol⁻¹
 x_i = molar fraction of compound i –
 z = axial coordinate cm

Greek Letters

α_i = adsorption/desorption coefficient –
 ε_b = bed porosity –
 ε_p = particle porosity –
 ν_i = stoichiometric coefficient of compound i –
 ρ = fluid phase density kg L⁻¹
 ρ_b = bulk density kg L⁻¹
 η_j = compound j viscosity g cm⁻¹ s⁻¹
 η_m = liquid phase viscosity g cm⁻¹ s⁻¹
 σ^2 = variance –
 τ = particle tortuosity –

REFERENCES

(1) *International Energy Outlook 2017*; DOE/EIA-0484(2017); U.S. Energy Information Administration, 2017.
 (2) *Renewables 2018 Global Status Report*; REN21, 2018.
 (3) Rashid, M. H. *Power electronics handbook*; Butterworth-Heinemann, 2017.
 (4) Fazal, M.; Haseeb, A.; Masjuki, H. Biodiesel feasibility study: an evaluation of material compatibility; performance; emission and engine durability. *Renewable Sustainable Energy Rev.* **2011**, *15* (2), 1314–1324.
 (5) Atabani, A. E.; Silitonga, A. S.; Badruddin, I. A.; Mahlia, T.; Masjuki, H.; Mekhilef, S. A comprehensive review on biodiesel as an alternative energy resource and its characteristics. *Renewable Sustainable Energy Rev.* **2012**, *16* (4), 2070–2093.

(6) Ma, F.; Hanna, M. A. Biodiesel production: a review. *Bioresour. Technol.* **1999**, *70* (1), 1–15.

(7) Tan, H.; Aziz, A. A.; Aroua, M. Glycerol production and its applications as a raw material: A review. *Renewable Sustainable Energy Rev.* **2013**, *27*, 118–127.

(8) Mota, C. J. A.; da Silva, C. X. A.; Rosenbach, N.; Costa, J.; da Silva, F. Glycerin Derivatives as Fuel Additives: The Addition of Glycerol/Acetone Ketal (Solketal) in Gasolines. *Energy Fuels* **2010**, *24* (4), 2733–2736.

(9) Melero, J. A.; Vicente, G.; Morales, G.; Paniagua, M.; Bustamante, J. Oxygenated compounds derived from glycerol for biodiesel formulation: Influence on EN 14214 quality parameters. *Fuel* **2010**, *89* (8), 2011–2018.

(10) da Silva, C. X. A.; Mota, C. J. A. The influence of impurities on the acid-catalyzed reaction of glycerol with acetone. *Biomass Bioenergy* **2011**, *35* (8), 3547–3551.

(11) Manjunathan, P.; Maradur, S. P.; Halgeri, A. B.; Shanbhag, G. V. Room temperature synthesis of solketal from acetalization of glycerol with acetone: Effect of crystallite size and the role of acidity of beta zeolite. *J. Mol. Catal. A: Chem.* **2015**, *396* (0), 47–54.

(12) Moreira, M. N.; Faria, R. P.; Ribeiro, A. M.; Rodrigues, A. E. Solketal Production from Glycerol Ketalization with Acetone: Catalyst Selection and Thermodynamic and Kinetic Reaction Study. *Ind. Eng. Chem. Res.* **2019**, *58* (38), 17746–17759.

(13) Nanda, M. R.; Yuan, Z.; Qin, W.; Ghaziaskar, H. S.; Poirier, M.-A.; Xu, C. C. Thermodynamic and kinetic studies of a catalytic process to convert glycerol into solketal as an oxygenated fuel additive. *Fuel* **2014**, *117* (0), 470–477 Part A.

(14) Deutsch, J.; Martin, A.; Lieske, H. Investigations on heterogeneously catalysed condensations of glycerol to cyclic acetals. *J. Catal.* **2007**, *245* (2), 428–435.

(15) Khayoon, M. S.; Hameed, B. H. Solventless acetalization of glycerol with acetone to fuel oxygenates over Ni-Zr supported on mesoporous activated carbon catalyst. *Appl. Catal., A* **2013**, *464–465* (0), 191–199.

(16) Khayoon, M.; Abbas, A.; Hameed, B.; Triwahyono, S.; Jalil, A.; Harris, A.; Minett, A. Selective Acetalization of Glycerol with Acetone Over Nickel Nanoparticles Supported on Multi-Walled Carbon Nanotubes. *Catal. Lett.* **2014**, *144* (6), 1009–1015.

(17) Vicente, G.; Melero, J. A.; Morales, G.; Paniagua, M.; Martín, E. Acetalisation of bio-glycerol with acetone to produce solketal over sulfonic mesostructured silicas. *Green Chem.* **2010**, *12* (5), 899–907.

(18) Fan, C.-N.; Xu, C.-H.; Liu, C.-Q.; Huang, Z.-Y.; Liu, J.-Y.; Ye, Z.-X. Catalytic acetalization of biomass glycerol with acetone over TiO₂-SiO₂ mixed oxides. *React. Kinet., Mech. Catal.* **2012**, *107* (1), 189–202.

(19) Souza, T. E.; Padula, I. D.; Teodoro, M. M.; Chagas, P.; Resende, J. M.; Souza, P. P.; Oliveira, L. C. Amphiphilic property of niobium oxyhydroxide for waste glycerol conversion to produce solketal. *Catal. Today* **2015**, *254*, 83–89.

(20) Nair, G.; Adrijanto, E.; Alsalmeh, A.; Kozhevnikov, I.; Cooke, D.; Brown, D.; Shiju, N. Glycerol utilization: solvent-free acetalisation over niobia catalysts. *Catal. Sci. Technol.* **2012**, *2* (6), 1173–1179.

(21) Nanda, M. R.; Yuan, Z.; Qin, W.; Ghaziaskar, H. S.; Poirier, M.-A.; Xu, C. Catalytic conversion of glycerol to oxygenated fuel additive in a continuous flow reactor: Process optimization. *Fuel* **2014**, *128* (0), 113–119.

(22) Shirani, M.; Ghaziaskar, H. S.; Xu, C. C. Optimization of glycerol ketalization to produce solketal as biodiesel additive in a continuous reactor with subcritical acetone using Purolite® PD206 as catalyst. *Fuel Process. Technol.* **2014**, *124*, 206–211.

(23) Clarkson, J. S.; Walker, A. J.; Wood, M. A. Continuous Reactor Technology for Ketal Formation: An Improved Synthesis of Solketal. *Org. Process Res. Dev.* **2001**, *5* (6), 630–635.

(24) Roldán, L.; Mallada, R.; Fraile, J. M.; Mayoral, J. A.; Menéndez, M. Glycerol upgrading by ketalization in a zeolite membrane reactor. *Asia-Pac. J. Chem. Eng.* **2009**, *4* (3), 279–284.

- (25) Guiochon, G.; Felinger, A.; Shirazi, D. G.; Katti, A. M. *Fundamentals of preparative and nonlinear chromatography*; Academic Press: Amsterdam, The Netherlands, 2006.
- (26) Silva, V. M. T. M.; Rodrigues, A. E. Dynamics of a fixed-bed adsorptive reactor for synthesis of diethylacetal. *AIChE J.* **2002**, *48* (3), 625–634.
- (27) Graça, N. S.; Pais, L. S.; Silva, V. M. T. M.; Rodrigues, A. E. Thermal effects on the synthesis of 1,1-dibutoxyethane in a fixed-bed adsorptive reactor. *Chem. Eng. Technol.* **2012**, *35* (11), 1989–1997.
- (28) Regufe, M. J.; Faria, R. P. V.; Ribeiro, A. M.; Loureiro, J. M.; Rodrigues, A. E. Synthesis of the Biofuel Additive 1,1-Diethoxybutane in a Fixed-Bed Column with Amberlyst-15 Wet. *Chem. Eng. Technol.* **2016**, *39*, 1509.
- (29) Faria, R. P. V.; Pereira, C. S. M.; Silva, V. M. T. M.; Loureiro, J. M.; Rodrigues, A. E. Sorption enhanced reactive process for the synthesis of glycerol ethyl acetal. *Chem. Eng. J.* **2014**, *258* (0), 229–239.
- (30) Pereira, C. S. M.; Silva, V. M. T. M.; Rodrigues, A. E. Fixed bed adsorptive reactor for ethyl lactate synthesis: Experiments, modelling, and simulation. *Sep. Sci. Technol.* **2009**, *44* (12), 2721–2749.
- (31) Sainio, T.; Zhang, L.; Seidel-Morgenstern, A. Adiabatic operation of chromatographic fixed-bed reactors. *Chem. Eng. J.* **2011**, *168* (2), 861–871.
- (32) Ferreira, M. V.; Ribeiro, A. M.; Loureiro, J. M. Experimental and Simulation Studies of TAME Synthesis in a Fixed-Bed Reactor. *Ind. Eng. Chem. Res.* **2007**, *46* (4), 1105–1113.
- (33) Constantino, D. S. M.; Pereira, C. S. M.; Faria, R. P. V.; Ferreira, A. F. P.; Loureiro, J. M.; Rodrigues, A. E. Synthesis of butyl acrylate in a fixed-bed adsorptive reactor over Amberlyst 15. *AIChE J.* **2015**, *61* (4), 1263–1274.
- (34) Ziyang, Z.; Hidajat, K.; Ray, A. K. Determination of adsorption and kinetic parameters for methyl tert-butyl ether synthesis from tert-butyl alcohol and methanol. *J. Catal.* **2001**, *200* (2), 209–221.
- (35) Pera-Titus, M.; Bausach, M.; Tejero, J.; Iborra, M.; Fité, C.; Cunill, F.; Izquierdo, J. F. Liquid-phase synthesis of isopropyl tert-butyl ether by addition of 2-propanol to isobutene on the oversulfonated ion-exchange resin Amberlyst-35. *Appl. Catal., A* **2007**, *323*, 38–50.
- (36) Soto, R.; Oktar, N.; Fité, C.; Ramírez, E.; Bringué, R.; Tejero, J. Adsorption of C1-C4 alcohols, C4-C5 isoolefins, and their corresponding ethers over Amberlyst 35. *Chem. Eng. Technol.* **2017**, *40* (5), 889–899.
- (37) Seidel-Morgenstern, A. Experimental determination of single solute and competitive adsorption isotherms. *Journal of Chromatography A* **2004**, *1037* (1), 255–272.
- (38) Glueckauf, E. Theory of chromatography. Part 10. Formulae for diffusion into spheres and their application to chromatography. *Trans. Faraday Soc.* **1955**, *51* (0), 1540–1551.
- (39) Wilson, E. J.; Geankoplis, C. J. Liquid Mass Transfer at Very Low Reynolds Numbers in Packed Beds. *Ind. Eng. Chem. Fundam.* **1966**, *5* (1), 9–14.
- (40) Scheibel, E. G. Correspondence. Liquid Diffusivities. Viscosity of Gases. *Ind. Eng. Chem.* **1954**, *46* (9), 2007–2008.
- (41) Perkins, L. R.; Geankoplis, C. J. Molecular diffusion in a ternary liquid system with the diffusing component dilute. *Chem. Eng. Sci.* **1969**, *24* (7), 1035–1042.
- (42) Kano, M. R.; Bae, Y.; Iwata, C.; Morishita, Y.; Yashiro, M.; Oka, M.; Fujii, T.; Komuro, A.; Kiyono, K.; Kaminishi, M.; Hirakawa, K.; Ouchi, Y.; Nishiyama, N.; Kataoka, K.; Miyazono, K. Improvement of cancer-targeting therapy, using nanocarriers for intractable solid tumors by inhibition of TGF- β signaling. *Proc. Natl. Acad. Sci. U. S. A.* **2007**, *104* (9), 3460–3465.
- (43) Mazzotti, M.; Neri, B.; Gelosa, D.; Morbidelli, M. Dynamics of a Chromatographic Reactor: Esterification Catalyzed by Acidic Resins. *Ind. Eng. Chem. Res.* **1997**, *36* (8), 3163–3172.
- (44) Lode, F.; Houmard, M.; Migliorini, C.; Mazzotti, M.; Morbidelli, M. Continuous reactive chromatography. *Chem. Eng. Sci.* **2001**, *56* (2), 269–291.
- (45) Pöpken, T.; Götze, L.; Gmehling, J. Reaction kinetics and chemical equilibrium of homogeneously and heterogeneously catalyzed acetic acid esterification with methanol and methyl acetate hydrolysis. *Ind. Eng. Chem. Res.* **2000**, *39* (7), 2601–2611.
- (46) Bozek-Winkler, E.; Gmehling, J. Transesterification of methyl acetate and n-butanol catalyzed by Amberlyst 15. *Ind. Eng. Chem. Res.* **2006**, *45* (20), 6648–6654.
- (47) Gandi, G. K.; Silva, V. M. T. M.; Rodrigues, A. E. Synthesis of 1,1-Dimethoxyethane in a Fixed Bed Adsorptive Reactor. *Ind. Eng. Chem. Res.* **2006**, *45* (6), 2032–2039.
- (48) Efron, B.; Tibshirani, R. J. *An Introduction to the Bootstrap*; CRC Press, 1994.
- (49) Joshi, M.; Kremling, A.; Seidel-Morgenstern, A. Model based statistical analysis of adsorption equilibrium data. *Chem. Eng. Sci.* **2006**, *61* (23), 7805–7818.